Article

Two 2D Layered P$_4$Mo$_6$ Clusters with Potential Bifunctional Properties: Proton Conduction and CO$_2$ Photoreduction

Ze-Yu Du, Zhang Chen, Run-Kun Kang, Ye-Min Han, Jie Ding, Jia-Peng Cao, Wei Jiang, Min Fang, Hua Mei,* and Yan Xu*

Read Online

ACCESS | Metrics & More | Article Recommendations | SI Supporting Information

ABSTRACT: Two hourglass-type molybdophosphate hybrids with the formulas $[Cd(H_2O)_2DABT]_4[Cd(H_7P_4Mo_6O_{31})_2]\cdot19H_2O$ (**1**) and $(C_2H_5OH)(C_3H_5N_2)_6[Co_3(H_6P_4Mo_6O_{31})_2]\cdot H_2O$ (**2**) (DABT= 3,3′-diamino-5,5′-bis(1H-1,2,4-triazole)) have been successfully designed and synthesized via a hydrothermal method. Structure analysis revealed that the inorganic moieties in compounds **1** and **2** are made up of hourglass-type $\{M[P_4Mo_6]_2\}$ (M = Cd/Co) structure, which were constructed by two (P$_4$Mo$_6$) units with single transition metal (TM) (Cd/Co) atom as the central metal. The $\{M[P_4Mo_6]_2\}$ (M = Cd/Co) structures were then further connected by TM to constitute a 2D layered structure. Surprisingly, under the condition of 60 °C and 98% RH, compounds **1** and **2** exhibited excellent proton conductivity of 1.35×10^{-3} and 3.78×10^{-3} S cm^{-1}, respectively. Furthermore, compound **2** can act as heterogeneous catalyst for CO$_2$ photoreduction, which indicates that it may be a bifunctional POM-based material with great promise.
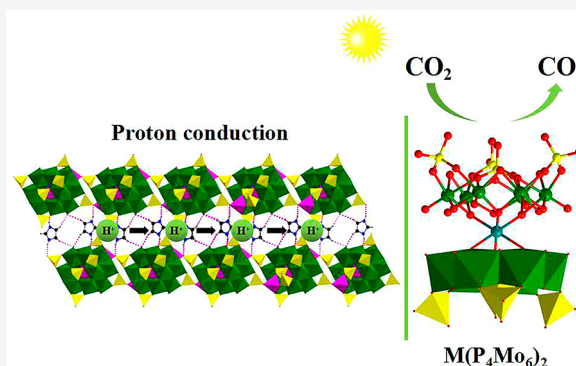
INTRODUCTION

Polyoxometalates (POMs), as one important member of metal oxides cluster materials with nanosized structural integrity, have triggered widespread attention from both academia and industry in recent years.[1−7] This phenomenon is not only due to their diverse structure, but also their potential practical values in various areas, such as optics, electrics, medicine, catalysis, and magnetism.[8−16] It is worth mentioning that in numerous kinds of POMs, there is a unique POM that called $[P_4Mo_6O_{28-x}(OH)_{3+x}]^{(9-x)-}$ cluster (P$_4$Mo$_6$) which exerts aesthetically fantastic structures.[17−19] Distinct from the classical POMs with {PO$_4$} groups in the center, such as Keggin and Dawson-type POMs, the P$_4$Mo$_6$ cluster has four {PO$_4$} groups located at the external of the cluster. Meanwhile, fully reduced Mo^V center and abundant phosphoric acid groups endow the P$_4$Mo$_6$ cluster with important electrical and catalytic properties.[20−22] Thus, based on above unique structure and potential application, the design and synthesis work of P$_4$Mo$_6$ cluster have been one of the significant tasks of researchers engaged in POM-based materials synthesis.

As is well-known, POM-based complexes displayed fabulous performances of proton conduction because of its high proton mobility supplied by oxygen-rich surface, abundant H-bonds, and water-retaining ability.[23−25] For example, Nakamura used the Keggin structural complex $\{H_3PM_{12}O_{40}\}$ (M = Mo, W) as the proton conducting material, which was the first report on POM-based proton conductive materials.[26] Among the reported

proton conductive materials based on POMs, the introduction of N-containing ligands (e.g., imidazole or triazole) could effectively improve proton conductivity via providing more mobile protons and smoothing transfer channel.[27,28] For instance, Lan's group synthesized the solid spherelike structural $(HIm)_{24}(NH_4)_{20}[Mo^{VI}_{72}Mo^V_{60}O_{372}(CH_3COO)_{30}(H_2O)_{72}]\cdot 90H_2O$ (Im = imidazole) and obtained excellent proton conductivity of 4.98×10^{-2} S cm^{-1}, which was one of the highest proton conductivities among POM-based proton conductive materials.[29] Recently, Liu and co-workers reported a P$_4$Mo$_6$ cluster with the formula $H_3\{[Na_2(H_2O)_2Na_4Fe^{III}_4(H_2O)_4(PO_4)]\text{-}[Na_{0.5}(H_2O)Fe^{II}_{0.5}Mo^V_4Mo^{VI}_2(OH)O_{14}(PO_4)_4]_4[Fe^{III}_4(H_2O)_8]\}\cdot 12H_2O$, exhibiting a high proton conduction performance of 1.33×10^{-2} S cm^{-1} because of the existence of rich phosphonic acid groups that have strong hydrophilicity and acidic property and vast proton donor and acceptor sites.[30] On the basis of the above-mentioned, the P$_4$Mo$_6$ cluster decorated with N-containing ligands (e.g., imidazole or triazole) may be an attractive candidate for proton conductive materials.
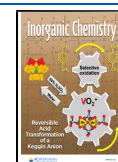
What's more, because of the potential applications of POMs in optical, catalytic, electrical, and magnetic properties, an increasing number of researchers pay attention to the synthesis of bifunctional POM-based materials in recent years.[31−35] As one of the most important parts of the catalytic properties, photocatalytic properties were investigated for the reported molybdophosphate hybrids,[22,36−38] from which it was disputable that the unique redox property and excellent photocatalytic activity made the P_4Mo_6 cluster a potential promising photocatalyst for the CO_2 photoreduction.

On the basis of above considerations, we successfully designed and synthesized two P_4Mo_6-based compounds $[Cd(H_2O)_2$-DABT$]_4[Cd(H_7P_4Mo_6O_{31})_2]\cdot19H_2O$ (**1**) and (C_2H_6O)-$(C_3H_5N_2)_6[Co_3(H_6P_4Mo_6O_{31})_2]\cdot H_2O$ (**2**). It is worth mentioning that the P_4Mo_6 cluster with abundant H-bonds endows compound **1** and **2** with excellent proton conductivity. Under the condition of 60 °C and 98% RH, the values of proton conductivity for compound **1** and **2** were 1.35×10^{-3} and 3.78×10^{-3} S cm^{-1}, respectively. Meanwhile, the protonated imidazole molecules in compound **2** could provide more mobile protons and smooth the proton transfer pathway, leading to higher proton conductivity than that of **1**. Besides, the photocatalytic performances of compound **2** exhibits the yield of CO was 5789 μmol g^{-1} under 8 h irradiation through examining the photocatalytic reduction of CO_2, which indicates the potential of bifunctional POM-based material.

■ EXPERIMENTAL SECTION

Materials and Physical Property Studies. 3,3′-Diamino-5,5′-bis(1H-1,2,4-triazole) (DABT) was prepared on the basis of a known literature method,[39] and other drugs and solvents were purchased with no further refinement. The content of C, H, and N were determined by a PerkinElmer 2400 elemental analyzer. PXRD analysis of two compounds was carried out on Smartlab TM 9KW diffractometer with monochromatized Cu−Kα (λ = 0.15418 nm) radiation, from 5 to 50°. FTIR spectrum was performed on Nicolet Impact 410 FTIR spectrometer through pressing KBr pellets, and the range was 400 to 4000 cm^{-1}. Thermogravimetric (TG) measurements of samples were completed on the Diamond thermogravimetric analyzer, and the temperature rose from 25 to 1000 °C in a N_2 atmosphere, with the heating rate of 10 °C min^{-1}. The UV−vis diffuse reflectance spectra was carried on SHIMADZU UV-2600 spectrophotometer, and the wavelength range was 200−800 nm.

Synthesis of Compounds. *Preparation of [Cd(H₂O)₂DABT]₄[Cd-(H₇P₄Mo₆O₃₁)₂]·19H₂O (1).* A mixture of Cd(OAc)$_2$·2H$_2$O (0.1332 g, 0.5 mmol), MoO$_3$ (0.0432 g, 0.3 mmol), L-alanine (0.0802 g, 0.9 mmol), DABT (0.0498 g, 0.3 mmol), H$_3$PO$_4$ (0.2 mL), and H$_2$O (8 mL) was stirred for 120 min, and the pH value was controlled at 2.5 using 2 M NaOH. Subsequently, the above mixture was put in a 25 mL stainless-steel autoclave and kept the autoclave at the temperature of 170 °C for 96 h. After falling to ordinary temperature, the red strip crystals of compound **1** were obtained (yield: 31% based on Mo). Elemental analysis result (%): C 4.45, H 2.26, N 10.42 (Calcd (%):C 4.49, H 2.20, N 10.48).

Preparation of (C₂H₆O)(C₃H₅N₂)₆[Co₃(H₆P₄Mo₆O₃₁)₂]·H₂O (2). A mixture of Co(OAc)$_2$·4H$_2$O (0.1245 g, 0.5 mmol), MoO$_3$ (0.0716 g, 0.5 mmol), imidazole (0.0666 g, 0.98 mmol), H$_2$O (4 mL), C$_2$H$_5$OH (4 mL), and tetrabutyl-ammonium hydroxide (1 mL) was stirred for 120 min, and the pH value was controlled at 4.5 using H$_3$PO$_4$. Subsequently, the above mixture was put in a 25 mL stainless-steel autoclave and kept the autoclave at the temperature of 180 °C for 120 h. After falling to ordinary temperature, the blue block crystals of compound **2** were obtained (yield: 35% based on Mo). Elemental analysis result (%): C 7.28, H 1.45, N 5.64 (Calcd (%):C 7.22, H 1.40, N 5.61).

X-ray Crystallography. The data of single-crystal X-ray diffraction for two compounds was performed on a Bruker SMART Apex II

CCD diffractometer with Mo−Kα radiation (λ = 0.71073 Å). The structures of two compounds were then analyzed using direct methods and refined by the full-matrix least-squares minimization through the SHELX-2018/3 program package. All the crystallographic information for compound **1** and **2** is listed in Table 1.

Table 1. Crystal Data and Structure Refinements for 1 and 2

	1	2
formula	$C_{16}H_{92}Cd_5Mo_{12}N_{32}O_{89}P_8$	$C_{20}H_{50}Co_3Mo_{12}N_{12}O_{64}P_8$
form wt	4118.25	3058.55
T (K)	296(2)	296(2)
cryst syst	monoclinic	triclinic
space group	$P2(1)/n$	$P\bar{1}$
a (Å)	13.7816(10)	12.999 (4)
b (Å)	22.0296(15)	13.862(4)
c (Å)	18.3385(12)	14.711(4)
α (deg)	90	95.522(3)
β (deg)	98.1640(10)	107.507(3)
γ (deg)	90	117.104(3)
V (Å^3)	5511.2(7)	2163.7(11)
Z	2	1
D_c (mg m^{-3})	2.482	2.347
μ (mm^{-1})	2.502	2.490
F (000)	3976	1471
θ range (deg)	1.454−25.010	1.510−25.001
limiting indices	$-16 \leq h \leq 16$,	$-15 \leq h \leq 14$,
	$-25 \leq k \leq 26$,	$-16 \leq k \leq 16$,
	$-21 \leq l \leq 21$	$-17 \leq l \leq 17$
no. of reflns collected	39019	14534
no. of independent reflns	9713 [R(int) = 0.0576]	7493 [R(int) = 0.0761]
data/restraints/ params	9713/211/790	7493/128/556
GOF	1.138	1.020
$R_1{}^a$	$R_1 = 0.0440$	$R_1 = 0.0494$
$wR_2{}^b[I > 2\sigma(I)]$	$wR_2 = 0.1233$	$wR_2 = 0.1310$
R_1, wR_2	$R_1 = 0.0599$	$R_1 = 0.0638$
(all data)	$wR_2 = 0.1299$	$wR_2 = 0.1398$

$^a R_1 = \Sigma||F_0| - |F_c||/\Sigma|F_0|$. $^b wR_2 = \Sigma[w(F_0^2 - F_c^2)^2]/\Sigma[w(F_0^2)^2]^{1/2}$.

■ RESULTS AND DISCUSSION

Synthesis. As is known to all, the hydrothermal method has been confirmed as an effective way to synthesize POM-based complexes. In the synthesis process, numerous factors have an influence on the growth of the crystal. To perfect the crystal quality, we optimize the kind of solvents, pH values, reaction time, and temperature to synthesize compounds **1** and **2**, leading to different preparation conditions of two compounds. Meanwhile, we chose N-containing ligands (DABT and imidazole) as building units to address the instability of POMs on the condition of high relative humidity and to supply more mobile proton.[40] Although L-alanine does not appear in the structure of compound **1**, we could not get the final products without adding L-alanine in the synthetic steps. In addition, it should be noted that two compounds all have high repeatability in the preparation process and can be distinctly distinguished by the shape and color, as shown in Figure S1.

Structure of [Cd(H₂O)₂DABT][Cd(H₇P₄Mo₆O₃₁)₂]·19H₂O (1). Single-crystal X-ray analysis showed that compound **1** crystallizes in the monoclinic $P2(1)/n$ space group. As shown in Figure 1d and Figure S2, compound **1** is composed of one
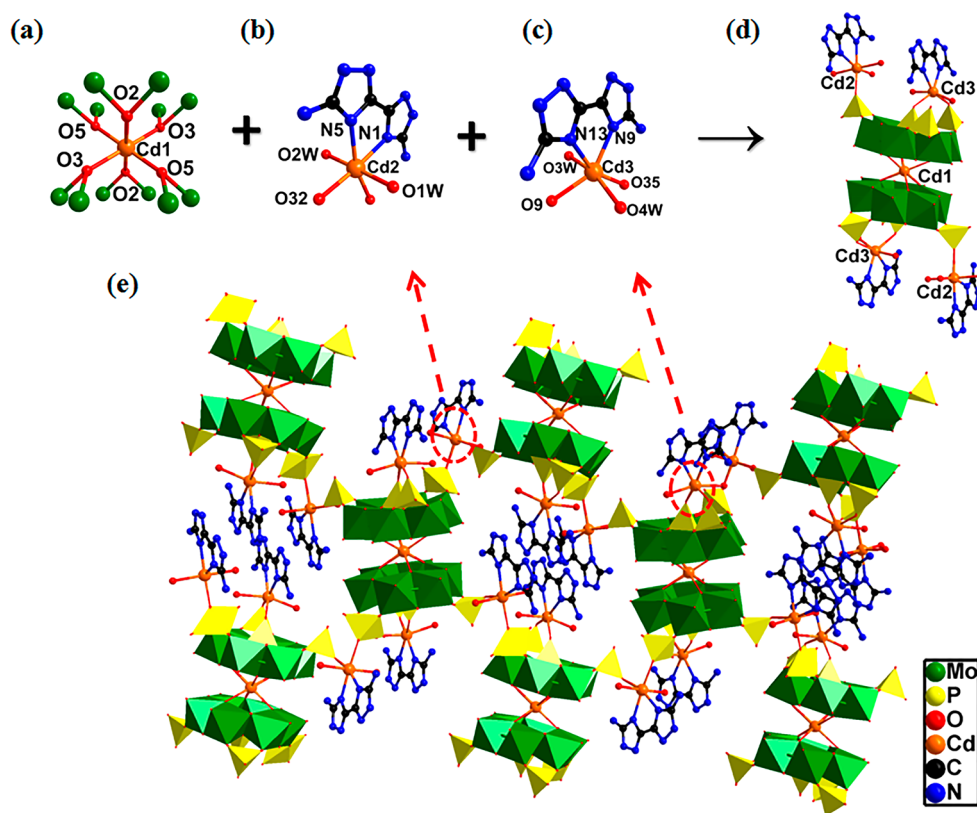
Figure 1. (a−c) Different coordination environment of Cd ions in **1**. (d) Ball−stick and polyhedral representations of the structural unit in **1**. (e) Ball−stick and polyhedral views of two-dimensional (2D) layer in **1**. The free water molecules and hydrogen atoms are omitted for clarity.
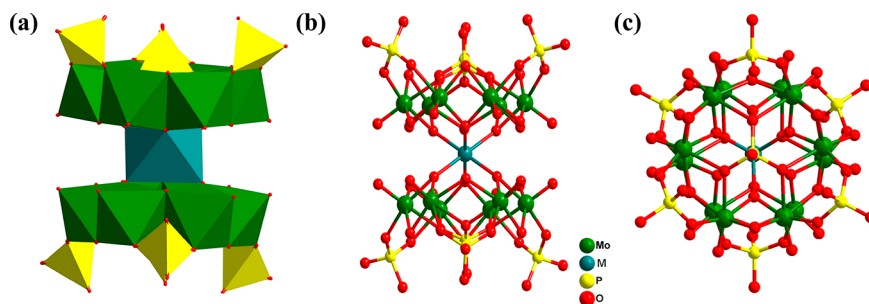

Figure 2. (a) Polyhedral presentation of the hourglass-type unit of $\{M[P_4Mo_6]_2\}$ (M = Cd in compound **1** and Co in **2**). (b) Side and (c) top views of the $\{M[P_4Mo_6]_2\}$ cluster.

$[Cd(H_7P_4Mo_6O_{31})_2]^{8-}$ anionic unit, four $[Cd(H_2O)_2DABT]^{2+}$ cations, and 19 free water molecules. The most basic unit of compounds **1** is (P_4Mo_6), which is formed by four $\{PO_4\}$ tetrahedral and six $\{MoO_6\}$ octahedral (Figure 2a). There are three types of Cd atoms with distinct coordination modes: the middle Cd1 (Figure 1a) and the pendant Cd2/Cd3 (Figure 1b, c). The Cd1 atom bridges two (P_4Mo_6) units via six μ_3-O atoms with a six-coordinated configuration to construct a hourglass-type $Cd[P_4Mo_6]_2$ dimer (Figure 2b, c). Meanwhile, the Cd2 and Cd3 atoms are all six-coordinated with two water oxygen, two nitrogen atoms from DABT, and two oxygen atoms from two $\{PO_4\}$ tetrahedral, respectively. The lengths of Cd2−O and Cd3−O bond vary from 2.227 (6) to 2.345 (8) Å, and the range of angles of O−Cd2−O and O−Cd3−O is from 83.1 (2) to 178.5 (2)° (Tables S1 and S2). Different from Cd3, the Cd2 atom can act as a linker to connect the two adjacent $Cd[P_4Mo_6]_2$ dimers in a two-dimensional (2D) arrangement (Figure 1e). Besides, the adjacent layers interact with each other by hydrogen

bonds of N−H···O (Table S5) to build up a 3D supramolecular structure, as shown in Figure S4.

Structure of $(C_2H_6O)(C_3H_5N_2)_6[Co_3(H_6P_4Mo_6O_{31})_2]·H_2O$ (2). Different from compound **1**, the compound **2** crystallizes in the triclinic $P\bar{1}$ space group. As shown in Figure S3, compound **2** consists of one $[Co_3(H_6P_4Mo_6O_{31})_2]^{6-}$ anionic unit, six protonated imidazole molecules, one free water, and one ethanol molecule. There are two kinds of Co atoms in compound **2**. Concretely, the Co1 atom as the center metal, connecting two (P_4Mo_6) units to form a hourglass-type $Co[P_4Mo_6]_2$ dimer unit (Figure 2b, c), and the Co2 is four-coordinated configuration that links four μ_2-O atoms (μ_2-O9, μ_2-O20, μ_2-O29, and μ_2-O31) from four $\{PO_4\}$ tetrahedral (Figure 3b, c). The lengths of Co2−O are in the range of 1.937 (6)−1.951 (5) Å, and the angle range of O−Co2−O varies from 98.7 (3) to 123.0 (2)° (Tables S3 and S4). Slightly different from compound **1**, every Co2 atom in compound **2** is connected with three adjacent $Co[P_4Mo_6]_2$ dimers to generate a two-dimensional (2D) structure (Figure 3c, d), and this layered
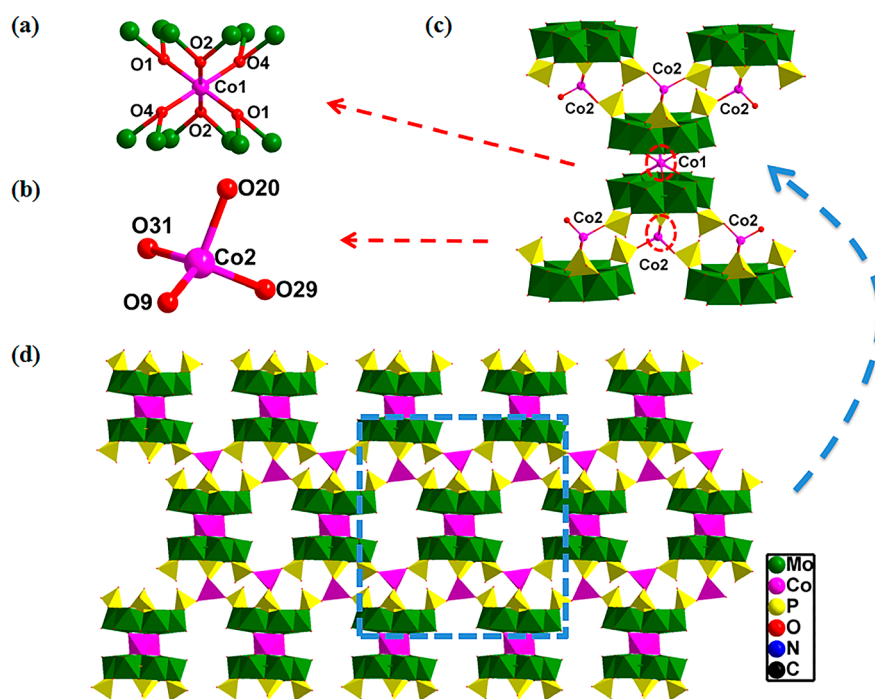
Figure 3. (a, b) Coordination environment of Co1 and Co2 ions in **2**; (c) ball-and-stick and polyhedral representations showing the linkage of Co ions in **2**; (d) polyhedral views of 2D layer in **2**. The hydrogen atoms, protonated imidazole molecules, free water, and ethanol molecules are omitted for clarity.

structure further connects with protonated imidazole by the H-bond of C−H···O and N−H···O (Table S6) to construct a 3D supramolecular structure (Figure S5), which may indicate that compound **2** has an excellent proton transfer ability due to the existence of abundant proton sources and hydrogen bonds.[41]

IR, XRD, and TG Analysis. As shown in Figures S6 and S7, the IR analysis of compound **1** and **2** showed some semblable stretching vibration peaks that are attributed to phosphomolybdate hybrids and organic ligands. Take compound **1** as an example; the characteristic peaks at 495 and 740 cm^{-1} can be thought to be ν (Mo−O−Mo).[42] The peaks at 955 and 1015 cm^{-1} are ascribed to ν (Mo = O) and ν (P−O), respectively. In addition, the peak at 1640 cm^{-1} belongs to the stretching vibrations of the C=N bonds from DABT, whereas the peaks at 1480, 2856, and 2925 cm^{-1} belong to the ν (C−H). Meanwhile, the strong peak at 3345 cm^{-1} is attributed to the stretching vibrations of O−H.

The XRD analysis of two compounds is shown in Figured S8 and S9. Notably, the measured values maintain high consistency with the corresponding theoretical spectra, which confirm that the two compounds have high phase purities.

The weight loss analysis of the two compounds is shown in Figures S13 and S14. For compound **1**, the weight loss curve consists of three parts. Originally, the weight loss of 12.17% with the temperature range is 25−190 °C, which is ascribed to the loss of coordination water and free water molecules (theoretical 11.8%). Because the structure of compound **1** is stable in this temperature range, the curve of the second part is almost unchanged between 190 and 340 °C. Then, with the further increase of temperature, the weight of compound **1** decreases 17.11% (theoretical 16.12%) because of the decomposition of organic ligands. In addition, the TG curve of compound **2** is similar to **1**, and the weight loss of 17.7% for **2** is

mainly attributed to the decomposition of imidazole and partial collapse of the skeleton (theoretical 15.64%).

Proton Conductivity. Proton conductivity of two compounds was investigated through an alternating current (AC) impedance spectrum. As shown in Figure 4, b, the conductivity of compound **1** and **2** was measured at 25 °C with different humidity to conform the correlation between relative humidity (RH) and proton conductivity. The conductivity of compound **1** was 1.13×10^{-9} S cm^{-1} at 40% RH, which could be considered as a negligible value. With the RH increasing to 98%, the proton conductivity of compound **1** increased to 1.55×10^{-4} S cm^{-1}, whereas compound **2** was 3.53×10^{-4} S cm^{-1}. Obviously, the increase in humidity is conducive to the increase in conductivity, so we examined the effect of different temperatures on the conductivity based on a RH of 98%, and the range of temperature was 25−60 °C with 5 °C intervals (Figure 4c, d). Under the conditions of 60 °C and RH of 98%, the conductivity value of compound **1** was 1.35×10^{-3} S cm^{-1}, whereas that of compound **2** was 3.78×10^{-3} S cm^{-1}, which was much higher than that of **1**. It should be noted that the proton conductivity of compound **2** was greater than those of most reported POM-based proton conductive materials (Table S7). What's more, the PXRD patterns (Figures S10 and S11) confirmed that compounds **1** and **2** are stable during the measurements.

Moreover, to strengthen our understanding of the proton conduction mechanism, we calculated the activation energy (E_a) of compound **1** was 0.53 eV and **2** was 0.57 eV at 98% relative humidity through the Arrhenius equation, as shown in Figure 5. Classically, the Grotthuss mechanism and the vehicle mechanism are extremely related to conductivity, which can be used to explain proton conduction. In general, the range of activation energy was 0.1−0.4 eV and mainly follows the Grotthuss mechanism, whereas the range of 0.5−0.9 eV mainly follows the vehicle mechanism, which may exit in two compounds.[43] For compound **1**, the number of hydrogen bonds
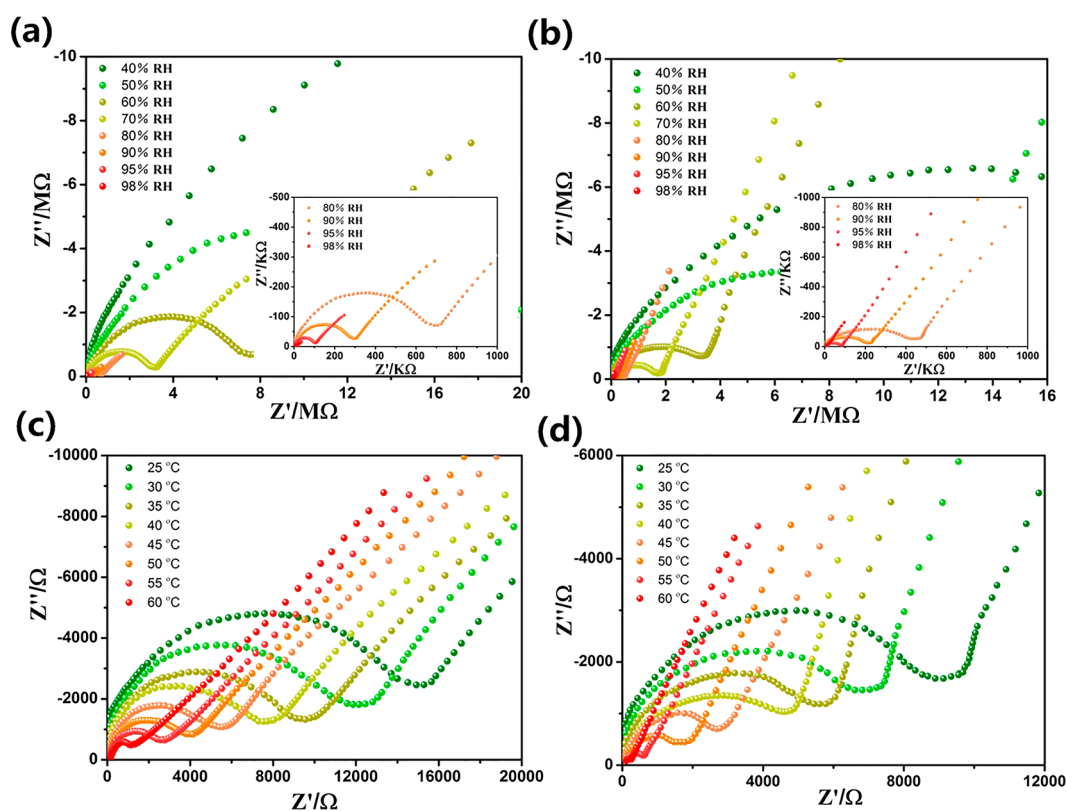
Figure 4. Impedance spectra of (a) compound **1** at 25 °C with different RH conditions, compound **2** at 25 °C with different RH conditions, (c) compound **1** at 98% RH with different temperatures, and (d) compound **2** at 98% RH with different temperatures.
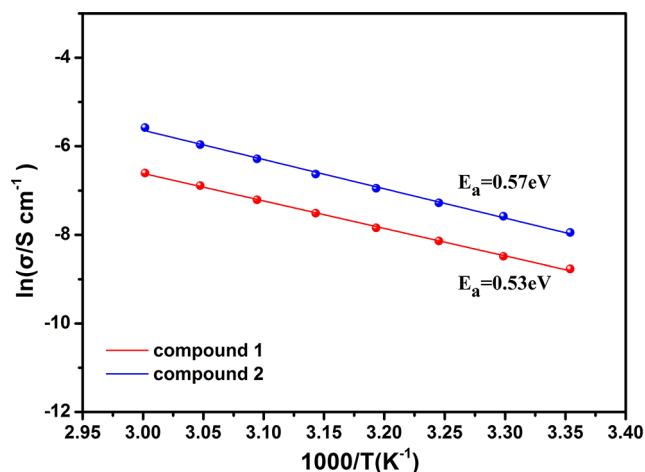

Figure 5. Arrhenius plots of proton conductivity for compound **1** (red) and **2** (blue) under 98% RH conditions.

could facilitate proton conduction, which was consistent with the Grotthuss mechanism, leading to low activation energy. Meanwhile, the free water molecules may receive protons from four-coordinated DABT ligands and transfer protons via self-diffusion, leading to a partial vehicle mechanism.[44] It can then be speculated that the protonated imidazole molecules of **2** are conducive to constructing continuous and rich hydrogen bonds, which could be used as the smooth pathway for proton migration and thus bringing about low activation energy. Simultaneously, because the channel in **2** was mainly occupied by free imidazole molecules, the guests have the possibility to move or rotate dynamically in the proton conduction, which was the reason for the high activation energy. Thus, the partial Grotthuss

mechanism and vehicular mechanism may all exit in two compounds.

The reason for the high proton conductivity and the difference between two compounds were utilized to further investigate through the results of structural analysis and activation energy. First, according to the test results, POMs possess an oxygen-rich surface, which could promote proton to alter pathway via transport on the oxygen-rich surface of POMs. Second, the existence of the phosphonic acid group is conducive to improving the proton conductivity by virtue of its strong hydrophilicity and acidic property and vast proton donor and acceptor sites. Third, abundant H-bonds of two compounds are instrumental in providing path for proton translocation. What's more, the presence of protonated imidazole molecules not only could easier provide more mobile protons but also administer a smooth proton transfer pathway in compound **2**,[27,45] resulting in higher proton conductivity than **1**. Hence, compared to **1**, the higher value of proton conductivity for compound **2** should be attributed to protonated imidazole molecules.

Photoreduction Property. The photocatalytic properties of compound **1** and **2** were investigated by examining the CO_2 photoreduction under visible-light illumination. In the system of CO_2 photocatalytic reduction, we put photocatalyst (10 mg) into a mixed solvent of triethanolamine and acetonitrile (1:4 v/v, 50 mL) and used $[Ru(bpy)_3]Cl_2 \cdot 6H_2O$ (11.3 mg) as photosensitizer. The whole reaction system was then irradiated through a Xe lamp, and the range of wavelength of light was greater than 420 nm. As shown in Figure 6a, when the reaction was carried out with a lack of photocatalyst, only traces of CO could be observed. In addition, the result also showed an extremely weak activity of the CO yield when we used compound **1** as photocatalyst (Figures S15 and S16). In contrast,
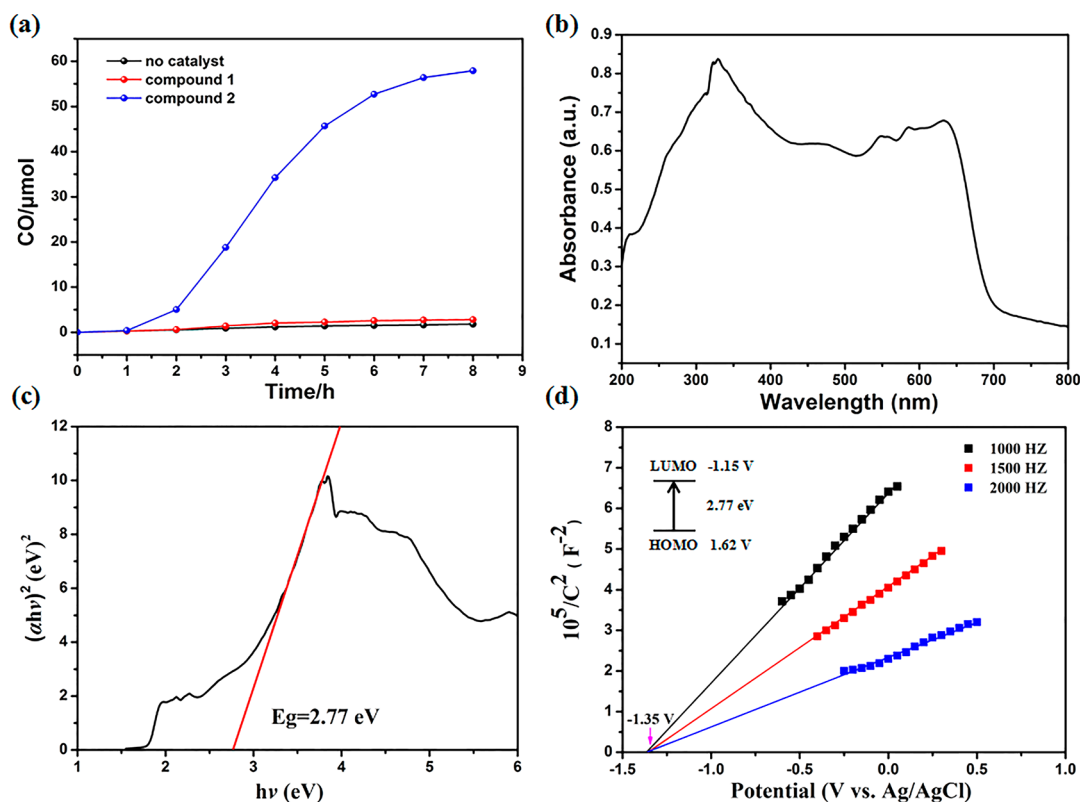
Figure 6. (a) Amount of CO produced as a function of the time of visible-light irradiation over compound **1** and **2**. (b) Solid-state UV−vis diffuse reflectance spectra of compounds **2**. (c) $(\alpha h\nu)^2$ vs $h\nu$ curve of compound **2**. (d) Mott−Schottky plots of compound **2**.

when we replaced compound **2** with **1**, the CO yield was obviously higher than previously (Figure S17). When the light time increases, the number of moles of CO gradually increase and the turnover number (TON) of CO was 17.7 under 8 h irradiation. Meanwhile, the relevant CO yield was 5789 μmol g^{-1}, which was greater than those of most reported POM-based photocatalysts (Table S8). In response to this phenomenon, we concluded that cobalt metal can provide more photocatalytic active sites for compound **2** to deliver high activity for CO_2 photoreduction.[46,47] After the reaction, the PXRD patterns of compound **2** confirmed that the photocatalysts are stable during the reaction and proved to be heterogeneous catalysts (Figure S12).

To further understand the CO_2 photoreduction mechanism, we investigated the solid-state UV−vis diffuse reflectance spectra and Mott−Schottky spots of compound **2** (Figure 6b, d). As shown in Figure 6b, the absorption edge of compounds **2** can reach nearly 700 nm, which may be attributed to the combination of coordinated Co atom and {P_4Mo_6} cluster.[48] Then, the band gap (E_g) of compound **2** was calculated via UV−vis data with the Kubelka−Munk eq (Figure 6c), and the value of band gap was 2.77 eV, which explained the excellent photocatalytic property for compound **2**. Meanwhile, Mott−Schottky plots with different frequencies were determined that the LUMO position was −1.15 V vs. NHE for compound **2** (Figure 6d). It should be noted that the LUMO position of compound **2** was more negative than the reduction potentials of CO_2 photoreduction ($CO/CO_2 = -0.53$ V vs. NHE), indicating that compound **2** could theoretically be a photocatalyst for CO_2 to CO reduction.

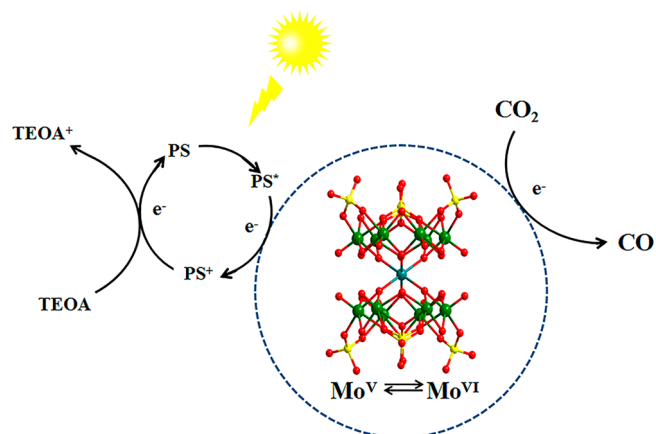On the basis of the results of CO_2 photoreduction experiments, we proposed a reaction mechanism about CO_2 photoreduction over compound **2** (Figure 7). First, the photosensitizer (PS) absorbs visible light to produce photoelectrons from the HOMO and transfers them to the catalyst via the matched LUMO positions. At the same time, TEOA plays the role of sacrificial agent in the system and consumes the photoinduced holes that generated from the valence band. Second, under the excitation of photoreduction, reductive {P_4Mo_6} clusters continuously transport electrons to the active metal sites. Third, the absorbed CO_2 molecules accept electrons from the catalyst and eventually turn into CO.

Figure 7. Proposed mechanism for the photoreduction of CO_2 to CO catalyzed by compound **2**.

CONCLUSION

In summary, two inorganic−organic hybrid materials based on the P_4Mo_6 cluster, possessing a two-dimensional (2D) structure,

have been synthesized under hydrothermal conditions. Under the condition of 60 °C and 98% RH, the excellent proton conductivities of compound **1** and **2** were 1.35×10^{-3} and 3.78×10^{-3} S cm^{-1}, respectively, resulting from abundant H-bonds that facilitate fast proton migration. For compound **2**, the introduction of protonated imidazole molecules provides more mobile protons and smooth proton transfer pathway in its structure, leading to higher proton conductivity than that of **1**. Notably, compound **2** can also act as a heterogeneous catalyst for CO_2 photoreduction and the CO yield was 5789 μmol g^{-1} under 8 h irradiation, which indicates it may be a decent bifunctional POM-based material with great promise.

ASSOCIATED CONTENT

ⓈI Supporting Information

The Supporting Information is available free of charge at https://pubs.acs.org/doi/10.1021/acs.inorgchem.0c01941.

> Impedance analysis, photocatalytic CO_2 reduction experiments, selected bond lengths and angles, hydrogen bonds, Tables S1–S8, and Figures S1–S17 (PDF)

Accession Codes

CCDC 2006831 and 2006832 contain the supplementary crystallographic data for this paper. These data can be obtained free of charge via www.ccdc.cam.ac.uk/data_request/cif, or by emailing data_request@ccdc.cam.ac.uk, or by contacting The Cambridge Crystallographic Data Centre, 12 Union Road, Cambridge CB2 1EZ, UK; fax: +44 1223 336033.

AUTHOR INFORMATION

Corresponding Author

Yan Xu − *College of Chemical Engineering, State Key Laboratory of Materials-Oriented Chemical Engineering, Nanjing Tech University, Nanjing 210009, P. R. China;* ⓘ orcid.org/0000-0001-6059-075X; Email: yanxu@njtech.edu.cn

Hua Mei − *College of Chemical Engineering, State Key Laboratory of Materials-Oriented Chemical Engineering, Nanjing Tech University, Nanjing 210009, P. R. China;* Email: meihua@njtech.edu.cn

Authors

Ze-Yu Du − *College of Chemical Engineering, State Key Laboratory of Materials-Oriented Chemical Engineering, Nanjing Tech University, Nanjing 210009, P. R. China*

Zhang Chen − *College of Chemical Engineering, State Key Laboratory of Materials-Oriented Chemical Engineering, Nanjing Tech University, Nanjing 210009, P. R. China*

Run-Kun Kang − *College of Chemical Engineering, State Key Laboratory of Materials-Oriented Chemical Engineering, Nanjing Tech University, Nanjing 210009, P. R. China*

Ye-Min Han − *College of Chemical Engineering, State Key Laboratory of Materials-Oriented Chemical Engineering, Nanjing Tech University, Nanjing 210009, P. R. China*

Jie Ding − *Jiangsu Collaborative Innovation Centre of Biomedical Functional Materials, Jiangsu College of Chemistry and Materials Science, Key Laboratory of New Power Batteries, Nanjing Normal University, Nanjing 210023, P. R. China*

Jia-Peng Cao − *College of Chemical Engineering, State Key Laboratory of Materials-Oriented Chemical Engineering, Nanjing Tech University, Nanjing 210009, P. R. China*

Wei Jiang − *College of Chemical Engineering, State Key Laboratory of Materials-Oriented Chemical Engineering, Nanjing Tech University, Nanjing 210009, P. R. China*

Min Fang − *Jiangsu Collaborative Innovation Centre of Biomedical Functional Materials, Jiangsu College of Chemistry and Materials Science, Key Laboratory of New Power Batteries, Nanjing Normal University, Nanjing 210023, P. R. China*

Complete contact information is available at:
https://pubs.acs.org/10.1021/acs.inorgchem.0c01941

Notes

The authors declare no competing financial interest.

REFERENCES

(1) Long, D. L.; Tsunashima, R.; Cronin, L. Polyoxometalates: Building Blocks for Functional Nanoscale Systems. *Angew. Chem., Int. Ed.* **2010**, *49*, 1736−1758.

(2) Miras, H. N.; Yan, J.; Long, D. L.; Cronin, L. Engineering Polyoxometalates with Emergent Properties. *Chem. Soc. Rev.* **2012**, *41*, 7403−7430.

(3) Du, D. Y.; Yan, L. K.; Su, Z. M.; Li, S. L.; Lan, Y. Q.; Wang, E. B. Chiral Polyoxometalate-Based Materials: From Design Syntheses to Functional Applications. *Coord. Chem. Rev.* **2013**, *257*, 702−717.

(4) Long, D. L.; Burkholder, E.; Cronin, L. Polyoxometalate Clusters, Nanostructures and Materials: from Self Assembly to Designer Materials and Devices. *Chem. Soc. Rev.* **2007**, *36*, 105−121.

(5) Lü, J.; Lin, J. X.; Zhao, X. L.; Cao, R. Photochromic Hybrid Materials of Cucurbituril and Polyoxometalates as Photocatalysts under Visible Light. *Chem. Commun.* **2012**, *48*, 669−671.

(6) Katsoulis, D. E. A Survey of Applications of Polyoxometalates. *Chem. Rev.* **1998**, *98*, 359−388.

(7) Luo, X. M.; Li, N. F.; Hu, Z. B.; Cao, J. P.; Cui, C. H.; Lin, Q. F.; Xu, Y. Polyoxometalate-Based Well-Defined Rodlike Structural Multifunctional Materials: Synthesis, Structure, and Properties. *Inorg. Chem.* **2019**, *58*, 2463−2470.

(8) Du, D. Y.; Qin, J. S.; Li, S. L.; Su, Z. M.; Lan, Y. Q. Recent Advances in Porous Polyoxometalate-Based Metal-Organic Framework Materials. *Chem. Soc. Rev.* **2014**, *43*, 4615−4632.

(9) AlDamen, M. A.; Clemente-Juan, J. M.; Coronado, E.; Martí-Gastaldo, C.; Gaita-Arino, A. Mononuclear Lanthanide Single-Molecule Magnets Based on Polyoxometalates. *J. Am. Chem. Soc.* **2008**, *130*, 8874−8875.

(10) Wang, S. S.; Yang, G. Y. Recent advances in polyoxometalate-catalyzed reactions. *Chem. Rev.* **2015**, *115*, 4893−4962.

(11) Craven, M.; Xiao, D.; Kunstmann-Olsen, C.; Kozhevnikova, E. F.; Blanc, F.; Steiner, A.; Kozhevnikov, I. V. Oxidative Desulfurization of Diesel Fuel Catalyzed by Polyoxometalate Immobilized on Phosphazene-Functionalized Silica. *Appl. Catal., B* **2018**, *231*, 82−91.

(12) Tian, A. X.; Yang, M. L.; Fu, Y. B.; Ying, J.; Wang, X. L. Electrocatalytic and Hg^{2+} Fluorescence Identifiable Bifunctional Sensors for a Series of Keggin Compounds. *Inorg. Chem.* **2019**, *58*, 4190−4200.

(13) Zhang, J.; Huang, Y.; Li, G.; Wei, Y. Recent Advances in Alkoxylation Chemistry of Polyoxometalates: From Synthetic Strategies, Structural Overviews to Functional Applications. *Coord. Chem. Rev.* **2019**, *378*, 395−414.

(14) Li, X. X.; Zhao, D.; Zheng, S. T. Recent Advances in POM Organic Frameworks and POM-Organic Polyhedra. *Coord. Chem. Rev.* **2019**, *397*, 220−240.

(15) Fu, H.; Qin, C.; Lu, Y.; Zhang, Z. M.; Li, Y. G.; Su, Z. M.; Li, W. L.; Wang, E. B. An Ionothermal Synthetic Approach to Porous Polyoxometalate-Based Metal-Organic Frameworks. *Angew. Chem., Int. Ed.* **2012**, *51*, 7985−7989.

(16) Müller, A.; Rehder, D.; Haupt, E. T. K.; Merca, A.; Bögge, H.; Schmidtmann; Heinze-Brückner, M. G. Artificial Cells: Temperature Dependent, Reversible Li[+]-Ion Uptake/Release Equilibrium at Metal Oxide Nanocontainer Pores. *Angew. Chem., Int. Ed.* **2004**, *43*, 4466−4470.

(17) Haushalter, R. C.; Lai, F. W. Synthesis of a New One-Dimensional Sodium Molybdenum Phosphate Polymer Structure of $[(H_3O)_2NaMo_6P_4O_{24}(OH)_7]^{2-}$. *Inorg. Chem.* **1989**, *28*, 2904−2905.

(18) Dong, Y. Y.; Dong, Z. M.; Zhang, Z. B.; Liu, Y. H.; Cheng, W. W.; Miao, H.; He, X. X.; Xu, Y. POM Constructed from Super-Sodalite Cage with Extra Large 24-Membered Channels: Effective Sorbent for Uranium Adsorption. *ACS Appl. Mater. Interfaces* **2017**, *9*, 22088−22092.

(19) Han, Z. G.; Xin, X.; Zheng, R.; Yu, H. T. Influence of Pb Element on the Catalytic Properties of {P$_4$Mo$_6$}-Polyoxometalate for Redox reactions. *Dalton Trans.* **2018**, *47*, 3356−3365.

(20) Gong, K. N.; Wang, W. J.; Yan, J. S.; Han, Z. G. Highly Reduced Molybdophosphate as a Noble-Metal-Free Catalyst for the Reduction of Chromium Using Formic Acid as a Reducing Agent. *J. Mater. Chem. A* **2015**, *3*, 6019−6027.

(21) Wang, W. J.; Han, Z. G.; Wang, X. X.; Zhao, C.; Yu, H. T. Polyanionic Clusters $[M(P_4Mo_6)_2]$ (M = Ni, Cd) as Effective Molecular Catalysts for the Electron-Transfer Reaction of Ferricyanide to Ferrocyanide. *Inorg. Chem.* **2016**, *55*, 6435−6442.

(22) Hou, L.; Zhang, Y. Q.; Ma, Y. Y.; Wang, Y. L.; Hu, Z. F.; Gao, Y. Z.; Han, Z. G. Reduced Phosphomolybdate Hybrids as Efficient Visible-Light Photocatalysts for Cr(VI) Reduction. *Inorg. Chem.* **2019**, *58*, 16667−16675.

(23) Cronin, L.; Muller, A. From Serendipity to Design of Polyoxometalates at the Nanoscale, Aesthetic Beauty and Applications. *Chem. Soc. Rev.* **2012**, *41*, 7333−7334.

(24) Miras, H. N.; Yan, J.; Long, D. L.; Cronin, L. Engineering Polyoxometalates with Emergent Properties. *Chem. Soc. Rev.* **2012**, *41*, 7403−7430.

(25) Banerjee, A.; Bassil, B. S.; Roschenthaler, G. V.; Kortz, U. Diphosphates and Diphosphonates in Polyoxometalate Chemistry. *Chem. Soc. Rev.* **2012**, *41*, 7590−7604.

(26) Nakamura, O.; Kodama, T.; Ogino, I.; Miyake, Y. High-Conductivity Solid Proton Conductors- Dodecamolybdophosphoric Acid and Dodecatungstophosphoric Acid Crystals. *Chem. Lett.* **1979**, *8*, 17−18.

(27) Cao, X.-L.; Xie, S.-L.; Li, S.-L.; Dong, L.-Z.; Liu, J.; Liu, X.-X.; Wang, W.-B.; Su, Z.-M.; Guan, W.; Lan, Y.-Q. A Well-Established POM-based Single-Crystal Proton-Conducting Model Incorporating Multiple Weak Interactions. *Chem. - Eur. J.* **2018**, *24*, 2365−2369.

(28) Cao, G. J.; Liu, J. D.; Zhuang, T. T.; Cai, X. H.; Zheng, S. T. A polyoxometalate−organic supramolecular nanotube with high chemical stability and proton-conducting properties. *Chem. Commun.* **2015**, *51*, 2048−2051.

(29) Liu, W. J.; Dong, L. Z.; Li, R. H.; Chen, Y. J.; Sun, S. N.; Li, S. L.; Lan, Y. Q. Different Protonic Species Affecting Proton Conductivity in Hollow Spherelike Polyoxometalates. *ACS Appl. Mater. Interfaces* **2019**, *11*, 7030−7036.

(30) Zhang, S.; Lu, Y.; Sun, X. W.; Li, Z.; Dang, T. Y.; Zhang, Z.; Tian, H. R.; Liu, S. X. Purely Inorganic Frameworks Based on Polyoxometalate Clusters with Abundant Phosphate Groups: Single-Crystal to Single-Crystal Structural Transformation and Remarkable Proton Conduction. *Chem. Commun.* **2020**, *56*, 391−394.

(31) Long, J.; Rouquette, J.; Thibaud, J. M.; Ferreira, R. A. S.; Carlos, L. D.; Donnadieu, B.; Vieru, V.; Chibotaru, L. F.; Konczewicz, L.; Haines, J.; Guari, Y.; Larionova, J. A High-Temperature Molecular Ferroelectric Zn/Dy Complex Exhibiting Single-Ion-Magnet Behavior and Lanthanide Luminescence. *Angew. Chem., Int. Ed.* **2015**, *54*, 2236−2240.

(32) Liu, M. J.; Yuan, J.; Zhang, Y. Q.; Sun, H. L.; Liu, C. M.; Kou, H. Z. Chiral Six-Coordinate Dy(III) and Tb(III) Complexes of an Achiral Ligand: Structure, Fluorescence, and Magnetism. *Dalton Trans.* **2017**, *46*, 13035−13042.

(33) Martin-Caballero, J.; San Jose Wery, A.; Reinoso, S.; Artetxe, B.; San Felices, L.; El Bakkali, B.; Trautwein, G.; Alcaniz-Monge, J.; Vilas, J. L.; Gutierrez-Zorrilla, J. M. A Robust Open Framework Formed by Decavanadate Clusters and Copper(II) Complexes of Macrocyclic Polyamines: Permanent Microporosity and Catalytic Oxidation of Cycloalkanes. *Inorg. Chem.* **2016**, *55*, 4970−4979.

(34) Zhai, Y. L.; Zhu, Z. J.; Zhu, C. Z.; Zhu, J. B.; Ren, J. T.; Wang, E. K.; Dong, S. J. Reversible Photo-Chem-Electrotriggered Three-State Luminescence Switching Based on Core-Shell Nanostructures. *Nanoscale* **2013**, *S*, 4344−4350.

(35) Cao, J. P.; Shen, F. C.; Luo, X. M.; Cui, C. H.; Lan, Y. Q.; Xu, Y. Proton Conductivity Resulting from Different Triazole-Based Ligands in Two New Bifunctional Decavanadates. *RSC Adv.* **2018**, *8*, 18560−18566.

(36) Xie, S. L.; Liu, J.; Dong, L. Z.; Li, S. L.; Lan, Y. Q.; Su, S. M. Hetero-Metallic Active Sites Coupled with Strongly Reductive Polyoxometalate for Selective Photocatalytic CO_2-to-CH_4 Conversion in Water. *Chem. Sci.* **2019**, *10*, 185−190.

(37) Tian, X. R.; Hou, L.; Wang, J. J.; Xin, X.; Zhang, H.; Ma, Y. Y.; Wang, Y. L.; Zhang, L. N.; Han, Z. G. Novel Fully Reduced Phosphomolybdates for Highly Efficient Removal of Inorganic Hexavalent Chromium and the Organic Dye Methylene Blue. *Dalton Trans.* **2018**, *47*, 15121−15130.

(38) Du, D. Y.; Qin, J. S.; Wang, T. T.; Li, S. L.; Su, Z. M.; Shao, K. Z.; Lan, Y. Q.; Wang, X. L.; Wang, E. B. Polyoxometalate-Based Crystalline Tubular Microreactor: Redox-Active Inorganic-Organic Hybrid Materials Producing Gold Nanoparticles and Catalytic Properties. *Chem. Sci.* **2012**, *3*, 705−710.

(39) Dippold, A. A.; Klapotke, T. M. Nitrogen-Rich Bis-1,2,4-Triazoles-A Comparative Study of Structural and Energetic Properties. *Chem. - Eur. J.* **2012**, *18*, 16742−16753.

(40) Li, J.; Cao, X. L.; Wang, Y. Y.; Zhang, S. R.; Du, D. Y.; Qin, J. S.; Li, S. L.; Su, Z. M.; Lan, Y. Q. The Enhancement on Proton Conductivity of Stable Polyoxometalate-Based Coordination Polymers by the Synergistic Effect of Multi Proton Units. *Chem. - Eur. J.* **2016**, *22*, 9299−9304.

(41) Su, J.; He, W.; Li, X. M.; Sun, L.; Wang, H. Y.; Lan, Y. Q.; Ding, M. N.; Zuo, J. L. High Electrical Conductivity in a 2D MOF with Intrinsic Superprotonic Conduction and Interfacial Pseudo-capacitance. *Matter* **2020**, *2*, 711−722.

(42) Li, W.; Zhu, J. N.; Shen, N. N.; Xiong, W. W.; Huang, X. Y. Assembling $[M(P_4Mo_6)_2]$ (M = Na, Mn, Na/Cu) Dimeric Clusters via Transition Metal/Sodium Ions into 0D to 3D Phosphomolybdates. *CrystEngComm* **2019**, *21*, 971−980.

(43) Ramaswamy, P.; Wong, N. E.; Shimizu, G. K. H. MOFs as Proton Conductors-Challenges and Opportunities. *Chem. Soc. Rev.* **2014**, *43*, 5913−5932.

(44) Zhang, F. M.; Dong, L. Z.; Qin, J. S.; Guan, W.; Liu, J.; Li, S. L.; Lu, M.; Lan, Y. Q.; Su, Z. M.; Zhou, H. C. Effect of Imidazole Arrangements on Proton-Conductivity in Metal-Organic Frameworks. *J. Am. Chem. Soc.* **2017**, *139*, 6183−6189.

(45) Wei, M. L.; Wang, X. X.; Duan, X. Y. Crystal Structures and Proton Conductivities of a MOF and Two POM-MOF Composites Based on Cu-II Ions and 2,2 '-Bipyridyl-3,3 '-Dicarboxylic Acid. *Chem. - Eur. J.* **2013**, *19*, 1607−1616.

(46) Lin, J. L.; Pan, Z. M.; Wang, X. C. Photochemical Reduction of CO_2 by Graphitic Carbon Nitride Polymers. *ACS Sustainable Chem. Eng.* **2014**, *2*, 353−358.

(47) Cao, Y. J.; Chen, S.; Luo, Q. Q.; Yan, H.; Lin, Y.; Liu, W.; Cao, L. L.; Lu, J. L.; Yang, J. L.; Yao, T.; Wei, S. Q. Atomic-Level Insight into Optimizing the Hydrogen Evolution Pathway over a Co$_1$-N$_4$ Single-Site Photocatalyst. *Angew. Chem., Int. Ed.* **2017**, *56*, 12191−12196.

(48) Du, J.; Ma, Y. Y.; Xin, X.; Na, H.; Zhao, Y. N.; Tan, H. Q.; Han, Z. G.; Li, Y. G.; Kang, Z. H. Reduced Polyoxometalates and Bipyridine Ruthenium Complex Forming a Tunable Photocatalytic System for High Efficient CO_2 Reduction. *Chem. Eng. J.* **2020**, *398*, 125518.